Theoretical and Applied Climatology
https://doi.org/10.1007/s00704-019-03076-4

ORIGINAL PAPER

Performance assessment of evapotranspiration estimated from different data sources over agricultural landscape in Northern India

Prashant K. Srivastava[1] · Prachi Singh[1] · R. K. Mall[1] · Rajani K. Pradhan[1,2] · Michaela Bray[3] · Akhilesh Gupta[4]

Received: 17 September 2018 / Accepted: 9 December 2019

Abstract
Accurate estimation of evapotranspiration is generally constrained due to lack of required hydrometeorological datasets. This study addresses the performance analysis of reference evapotranspiration (ETo) estimated from NASA/POWER, National Center for Environmental Prediction (NCEP) global reanalysis data before and after dynamical downscaling through the Weather Research and Forecasting (WRF) model. The state-of-the-art Hamon's and Penman-Monteith's methods were utilized for the ETo estimation in the Northern India. The performance indices such as bias, root mean square error (RMSE), and correlation (*r*) were calculated, which showed the values 0.242, 0.422, and 0.959 for NCEP data (without downscaling) and 0.230, 0.402, and 0.969 for the downscaled data respectively. The results indicated that after WRF downscaling, there was some marginal improvement found in the ETo as compared to the without downscaling datasets. However, a better performance was found in the case of NASA/POWER datasets with bias, RMSE, and correlation values of 0.154, 0.348, and 0.960 respectively. In overall, the results indicated that the NASA/POWER and WRF downscaled data can be used for ETo estimation, especially in the ungauged areas. However, NASA/POWER is recommended as the ETo calculations are less computationally expensive and easily available than performing WRF simulations.

1 Introduction

Evapotranspiration defined as the "combined loss of water from a given area, and during a specified period of time by evaporation from the soil surface and by transpiration from plants" (Thornthwaite 1948). It is considered as one of the most important components of the hydrological cycle (Mall and Gupta 2002; Srivastava et al. 2016). On the Earth surface, it has very important role in the context of water and energy balances as well as required in the irrigation and agriculture practices (Nag et al. 2014). In addition, evapotranspiration is required in many scientific disciplines to understand the underlying hydrological processes (Petropoulos et al. 2015; Petropoulos et al. 2016). However, in spite of the several efforts made by many government agencies, there are still lack of sufficient meteorological stations for measurement of reliable and accurate datasets for evapotranspiration (ETo) estimation.

Previously, indirect approaches are generally used for ETo measurements (Srivastava et al. 2017). One means of estimating ETo is through the use of a lysimeter, which determines the evapotranspiration by recording the amount of precipitation an area receives and the amount lost through the soil. However, due to high maintenance cost, time consumption, and lack of precise instrumentation, its implementation is not easy, especially for larger areas (Pandey et al. 2016). Nevertheless, there are a number of other methods developed in the past decades, which quantify ETo (Alkaeed et al. 2006; Djaman et al. 2015; Lang et al. 2017). Among them, the simplest approach was developed by Hamon (1960), which requires only temperature data for ETo calculation. In (2015), McCabe et al. used the

Electronic supplementary material The online version of this article (https://doi.org/10.1007/s00704-019-03076-4) contains supplementary material, which is available to authorized users.

✉ R. K. Mall
rkmall@bhu.ac.in

[1] DST-Mahamana Centre for Excellence in Climate Change Research, Institute of Environment and Sustainable Development, Banaras Hindu University, Varanasi, Uttar Pradesh 221005, India

[2] Faculty of Environmental Sciences, Czech University of Life Sciences Prague, Prague, Czech Republic

[3] University of Cardiff, Cardiff, Wales, UK

[4] Department of Science and Technology, New Delhi, India

monthly calibrated coefficient values to calculate the ETo and found that the mean monthly ETo (using Hamon's method) were close to the mean monthly free-water surface evaporation.

From many studies, the FAO-56 Penman-Monteith (PM) method is considered to be the most suitable indirect method for estimation of reference evapotranspiration (ETo). Cai et al. in 2007 used the daily real-time ETo in the field of water resources management. Kar et al. in 2016 compared the ETo, computed by eight different methods for the dry sub-humid agro-ecological region. They found that the estimated ETo calculated via the Penman-Monteith method provide a better estimate of ETo as compared to all the other methods. However, a major drawback of the PM method is that it demands several meteorological parameters (wind speed, humidity, sunshine hour, etc.), which may not be often available everywhere (Chen et al. 2005), could be due to the lack of availability of stations or missing values due to station poor maintenance (Pandey et al. 2016).

There were very few studies focused on the ETo estimation using the mesoscale model like MM5 (Mesoscale modelling system 5), Weather Research and Forecasting model combined with NASA/POWER datasets, etc. Some studies reported on the use of mesoscale models for estimation of ETo in different parts of the world (Falk et al. 2014; Lin et al. 2018; Srivastava et al. 2013, 2016). Ishak et al. (2010) have estimated the ETo over Brue catchment, southwestern England using the ECMWF ERA-40 reanalysis downscaled data through MM5 model. Silva et al. (2010) have investigated the potential use of numerical weather forecast obtained from MM5, as a proxy for surface meteorological data with specific objective to use it in the estimation of ETo over Maipo river basin. Later, Srivastava et al. (2013, 2016) used the WRF model to downscale the ECMWF and NCEP reanalyzed datasets over the Brue catchment and reported a better performance of ECMWF than NCEP downscaled datasets.

Despite the high importance of ETo in the field of hydrology and climatological studies, there are only a few studies available in the technical literature domain, which demonstrate the accuracy and performance of the ETo derived from the WRF model and NASA/POWER datasets, especially for the Indian regions. Therefore, this paper provides a detailed cross comparison of ETo estimated from different existing datasets—NCEP, WRF downscaled NCEP, and NASA/POWER over cropland by using Hamon's and Penman-Monteith's methods in the Northern India. Further detailed analysis with respect to seasonality is also provided to determine the appropriateness of these methods of deriving ETo with regard to seasonal variability. The outcomes of the study can be used by the agricultural, meteorological, and hydrological departments to improve their forecast ability.

2 Materials and methodology

2.1 Study area

The study area consists of agricultural landscape, geographically lies between 25° 14′ 54.94″ N to 25° 17′ 06.57″ N and 82° 58′ 30″ E to 83° 00′ 35″ E in the Northern India, considered as food bowl of the country. Topographically, it is located on higher ground with mean elevation of 80.71 m (Cai et al. 2009). Being situated in the Indo-Gangetic plain, the land is composed of very fertile alluvial soil deposited by Rivers Ganga and Varuna. Climatically, the area is sub-humid type, characterized by hot summer, cold season, and pleasant monsoon. The temperature varies from 22 to 46 °C in summer and may drop below 5 °C in winter season. June is the hottest month with the mean temperature around 35 °C and mid-December to January is the coldest month (< 5 °C). The mean annual rainfall is 1036 mm, whereas about 90% of the total rainfall takes place in monsoon season from June to September. Geologically, the study area is characterized by Gangetic alluvium formed by the deposition sediment by river Ganga and its tributaries. The observational temperature dataset (2009–2016) is used for the estimation of ETo provided by the Department of Agriculture, Banaras Hindu University, India. In addition, three sets of reanalyzed data sets—NCEP, WRF downscaled NCEP (hereafter WRF-NCEP), and NASA-POWER—were collected and used for the estimation of ETo for the time period 2009–2016 and compared with the observed ETo. An overview of the methodology used in the present study is shown in Fig. 1.

2.2 Weather research and forecasting model

The WRF model was developed by scientists at the National Center for Atmospheric Research (NCAR), National Centers for Environmental Prediction (NCEP), the National Oceanic and Atmospheric Administration (NOAA), the Naval Research Laboratory, the Earth System Research Laboratory, the University of Oklahoma, the U.S. Air Force, and the Federal Aviation Administration (FAA). The Weather Research Forecasting (WRF) is a next-generation, non-hydrostatic, and mesoscale modeling system. This numerical weather prediction model and data assimilation system are used in atmospheric research and operational application (Skamarock et al. 2001). WRFI is useful for various applications such as assimilation of meteorological datasets, air quality modeling, and downscaling climate simulations as well as the atmosphere research (Mohan and Sati 2016). It comprises of ARW

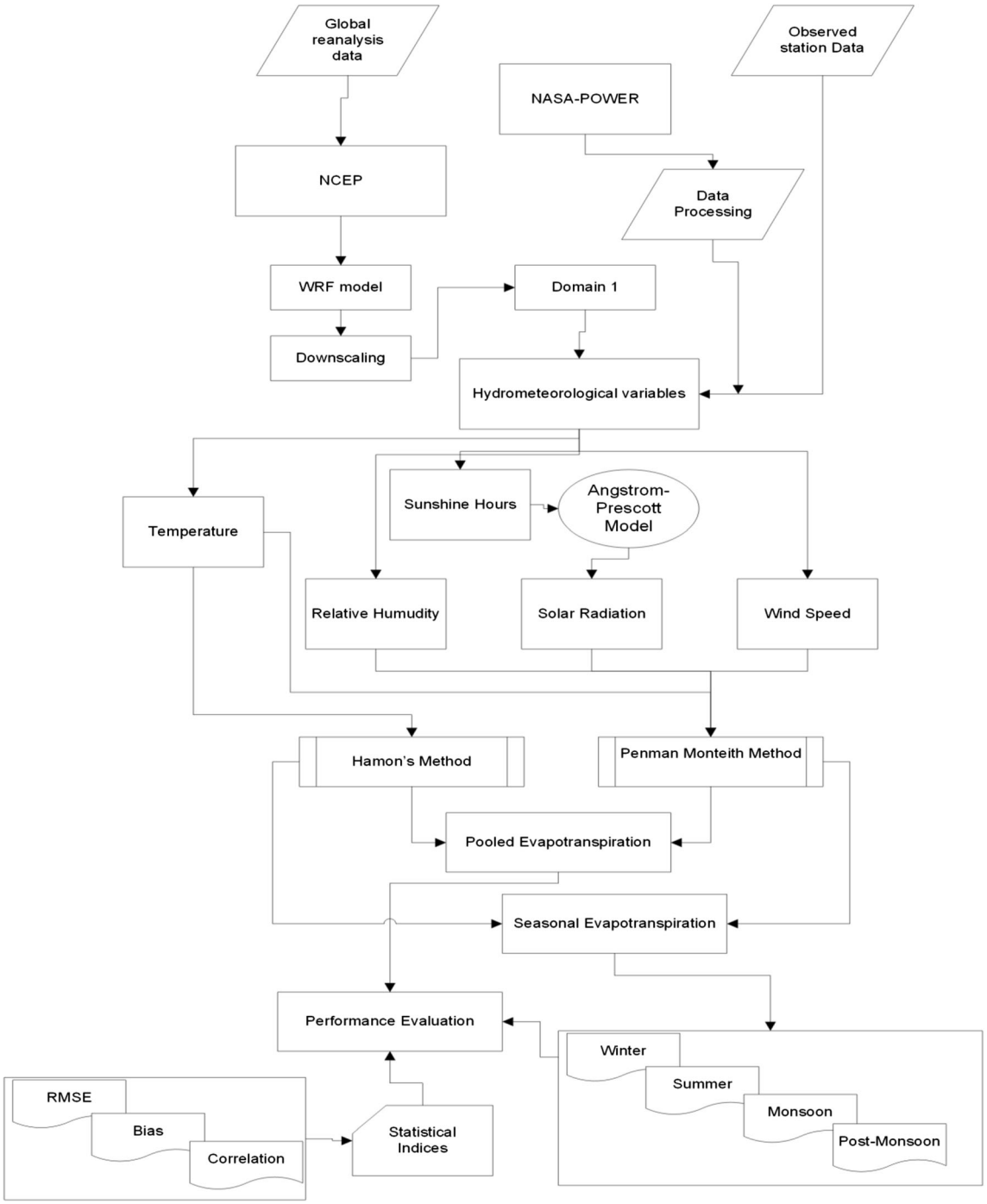

Fig. 1 Flowchart of the methodology

(Advance Research WRF) and NMM (Non-Hydrostatic Mesoscale model) cores (Schwartz et al. 2009; Srivastava et al. 2016). In this study, WRF is used to downscale the NCEP data over the selected region in Northern India. Meteorological data downscaled from the WRF model was used for calculation of ETo. Derived ETo is compared with the observed dataset obtained from the station. For microphysics, we used WSM 6 - class graupel scheme inbuilt with ice, snow, and graupel processes. The graupel scheme is highly suitable for high-resolution simulations and developed at the National Center for Atmospheric Research (NCAR) (Hong and Lim 2006). The long-wave radiation RRTM (Rapid Radiative Transfer Model) scheme is used because of its high efficiency (Mlawer et al. 1997). The Dudhia scheme is used as it is efficient for cloud and clear-sky absorption and scattering (Dudhia 1988). In surface layer option, Monin-Obukhov similarity scheme is used. YSU scheme is selected to constitute near surface weather operations (Kim and Wang 2011).

2.3 NASA/POWER and NCEP datasets

In this study, the hydrometeorological variables were estimated using the NCEP data directly, after downscaling of NCEP using WRF (WRF-NCEP) and NASA/POWER as well as from ground-based station. The Worldwide Energy Resources (NASA/POWER) project was initiated in 2003, which is an upgrade to the surface meteorology and solar energy (SSE) project. The NASA/POWER Release-8 provides the meteorological data on a global grid scale with spatial resolution of 0.5° × 0.5°. The NASA/POWER data was developed by using the satellite, ground observation, windsondes, modeling, and data assimilation techniques. The meteorological data sets are taken from NASA Modern Era Retro-Analysis for Research and Applications (MERRA-2) assimilation model and from Goddard Earth Observing System Model, version 5.12.4 (GEOS) assimilation model. GEOS is a system of models integrated using the Earth System Modeling Framework (ESMF) being developed in the GMAO (Global Modeling and Assimilation Office) to support NASA's earth science research in data analysis, climate and weather prediction, and basic research. In this study, the meteorological variables were downloaded from the NASA/POWER website (https://power.larc.nasa.gov/) for the time span of 2009–2016. In addition, the global NCEP FNL (Final) reanalysis dataset from 2009 to 2016 was used for the estimation of ETo. The NCEP-NCAR global reanalysis data set is an assimilated dataset developed using a state of art analysis forecast system (Kalnay et al. 1996). The NCEP datasets with 1° × 1° grids are available at every 6 h and can be downloaded from the website (http://rda.ucar.edu/). The NCEP data is available from 1948 to present and updated continuously.

2.4 Evapotranspiration estimation

2.4.1 Hamon's method

In this study, potential evapotranspiration (PET) is calculated using Hamon's equation. Hamon equation uses only the temperature and is a simple and robust method for calculating evapotranspiration (McCabe et al. 2015). PET is calculated using downscaled and non-downscaled NCEP reanalysis data and compared with the observed ETo. As the area under consideration is cropland and there is adequate availability of water, the ETo values can be considered closer to the PET values.

Hamon equation can be expressed as follows:

$$PET = K{*}0.165{*}216.7{*}N{*}\left(\frac{e_s}{T+273.3}\right) \tag{1}$$

where PET is in mm day^{-1}, K is the proportionality coefficient, N is the daytime length (x/12 h), e_s is the saturation vapor pressure (hPa), and T is the average monthly temperature.

$$e_s = 6.108_e\left(\frac{17.27T}{T+273.3}\right) \tag{2}$$

2.4.2 Penman-Monteith method

The Food and Agricultural Organization-56 (FAO) Penman-Monteith method was considered to estimate daily ETo (Monteith 1965; Penman 1956). The FAO-56 PM method is recommended as the best method for ETo estimation for all types of climates (Allen et al. 1998) and the equation for estimation of daily ETo can be expressed as

$$ETo = \frac{0.408\Delta(R_n - G) + \gamma\frac{900}{T+273}u_2(e_s - e_a)}{\Delta + \gamma(1+0.34u_2)} \tag{3}$$

where ETo rate is in mm day^{-1}, R_n is the net radiation at the crop surface (MJ m^{-2} day^{-1}), T is the mean air temperature (°C), u_2 is the wind speed (m s^{-1}) at 2 m above the ground, e_s is the saturation vapor pressure (kPa), e_a is the actual vapor pressure, e_s-e_a is the saturation vapor pressure deficit (kPa), Δ is the slope vapor pressure curve (kPa °C^{-1}), γ is the psychrometric constant (kPa °C^{-1}), and G is the soil heat flux density (MJ m^{-2} day^{-1}).

$$\Delta = \frac{4098\left[0.6108\ \exp\left(\frac{17.27T}{T+237.3}\right)\right]}{(T+237.3)^2} \tag{4}$$

where T is the air temperature and $e = 2.7183$ (base of natural logarithm).

For the calculation of R_n (net radiation), R_a (extraterrestrial radiation) value is required. R_a can be calculated using the following equation:

$$R_a = \frac{24(60)}{\pi}G_{sc}d_r[(\omega_s\sin\phi\sin\delta) + (\cos\phi\cos\delta\sin\omega_s)] \tag{5}$$

where R_a is the extraterrestrial radiation (MJ m^{-2} day^{-1}), G_{sc} solar constant = 0.0820 MJ m^{-2} min^{-1}, d_r inverse relative distance Earth-Sun, w_s sunset hour angle [radian], j = latitude [radian], d = solar decimation [radian] (Zotarelli et al. 2010).

2.5 Angstrom-Prescott model

Since solar radiation is not available for the study area, to avoid this difficulty, the FAO56 suggested Angstrom-Prescott (AP) equation, which is a simple straightforward method to predict the daily global solar radiation and therefore considered here to calculate the monthly daily extraterrestrial

radiation (Podder et al. 2014). The equation is given as follows:

$$H_0 = \frac{24}{\pi} G_{sc}\left(1 + \frac{360n}{365}\right) \times \left(\cos\phi\cos\delta\sin\omega_s + \frac{\pi\omega_s}{180^{\circ}}\sin\phi\sin\delta\right) \quad (6)$$

where H_0 is the solar radiation, G_{sc} is the solar constant (1.361 kW/m^2), n is the daily maximum sunshine duration in hour, ϕ is the latitude in degree, δ is the solar declination in degree, and ω_s is the sunset hour angle in degree.

3 Results and discussion

3.1 Evaluation of hydrometeorological variables

From NCEP, WRF-NCEP, and NASA/POWER data sets, weather variables were extracted for ETo estimation. Temporal variations of temperature are shown in Fig. 2, while combined (pooled) performance statistics are shown in Fig. 3. The three statistical indices correlation (r), RMSE, and bias are calculated between NCEP, WRF-NCEP, and NASA/POWER estimated temperature and compared with the ground-based observations. As shown in Fig. 3, we can observe a gradual increment in the temperature data, when proceeding from the winter to summer seasons. Among three datasets, the WRF-NCEP data has the highest correlation ($r = 0.976$), followed by NCEP ($r = 0.971$) and NASA/POWER (0.969), which indicates a close agreement of temperature with ground observations. However, in terms of RMSE and bias, the NASA/POWER has shown a better performance followed by WRF-NCEP and NCEP estimated temperatures (Table 1). Some outliers can be seen in Fig. 3; a detailed investigation revealed that during those days, sporadic rainfall occurs in the area, which is well captured by the meteorological station but not detected in any of the simulated products. These scattered or isolated rainfall in the summer season caused a sudden cooling down of the land surface and

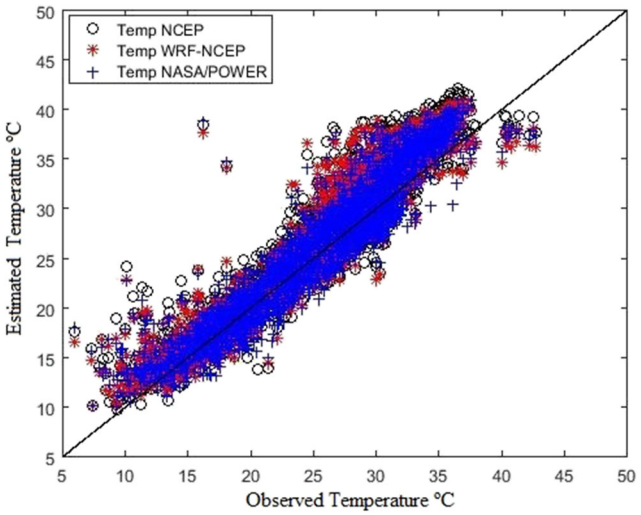

Fig. 3 Scatter plot representing the variations among WRF-NCEP, NCEP, and NASA/POWER temperature with observed datasets

leads to lowering of the temperature during those days. Other localized factors such as irrigation practices at specific intervals in the area also caused a reduction in the temperature, but not detected in the global reanalysis products used in this study. These sharp variations are not properly captured by NASA/POWER, NCEP, and WRF-NCEP, and thus, an overestimation can be seen in Fig. 3. Further, Fig. 4 shows the performance of estimated temperature on a seasonal basis and with observed dataset. From Fig. 2, temperature estimated from different sources showed a close agreement with the ground-based observations. In winter, in terms of correlation, the NCEP temperature (0.948) has shown a good performance as compared to the WRF-NCEP (0.940) and NASA/POWER (0.934) datasets.

However, in terms of bias and RMSE, the WRF-NCEP downscaled temperature reveals better results than the other datasets. As compared to winter, in summer, the estimated temperature is overestimating most of the time. Interestingly in summer, the NASA/POWER estimated temperature has the highest correlation ($r = 0.966$) followed by WRF-NCEP ($r =$

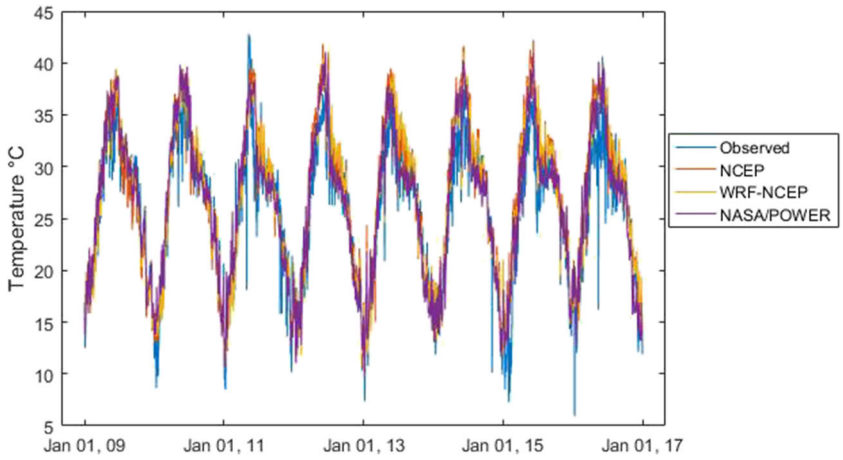

Fig. 2 Temporal plot for WRF-NCEP, NCEP, and NASA/POWER daily temperature with observed datasets

Table 1 Performance statistics of the seasonal and pooled daily temperature

Variables	NCEP			WRF-NCEP			NASA/POWER		
	r	RMSE	Bias	*r*	RMSE	Bias	*r*	RMSE	Bias
Pooled temperature	0.971	2.233	1.333	0.976	2.134	1.210	0.969	1.914	0.826
Winter temperature	0.948	1.236	0.926	0.940	0.830	0.320	0.934	1.457	1.175
Summer temperature	0.930	3.249	2.829	0.957	2.429	2.010	0.966	2.655	2.402
Monsoon temperature	0.883	2.284	1.572	0.807	2.697	2.290	0.888	1.850	0.605
Post-monsoon temperature	0.962	1.156	− 0.215	0.947	1.449	− 0.430	0.965	1.263	−0.682

0.957) and NCEP (0.930). In the WRF-NCEP estimated temperature, a comparatively smaller RMSE and bias was obtained than the other datasets. During the monsoon periods, a poor performance was observed in estimated temperature especially in the WRF-NCEP and NCEP compared to the observations, while the NASA/POWER showed a better result. The frequent and abrupt changes in the weather variables in monsoon season due to rainfall, especially in the Indian

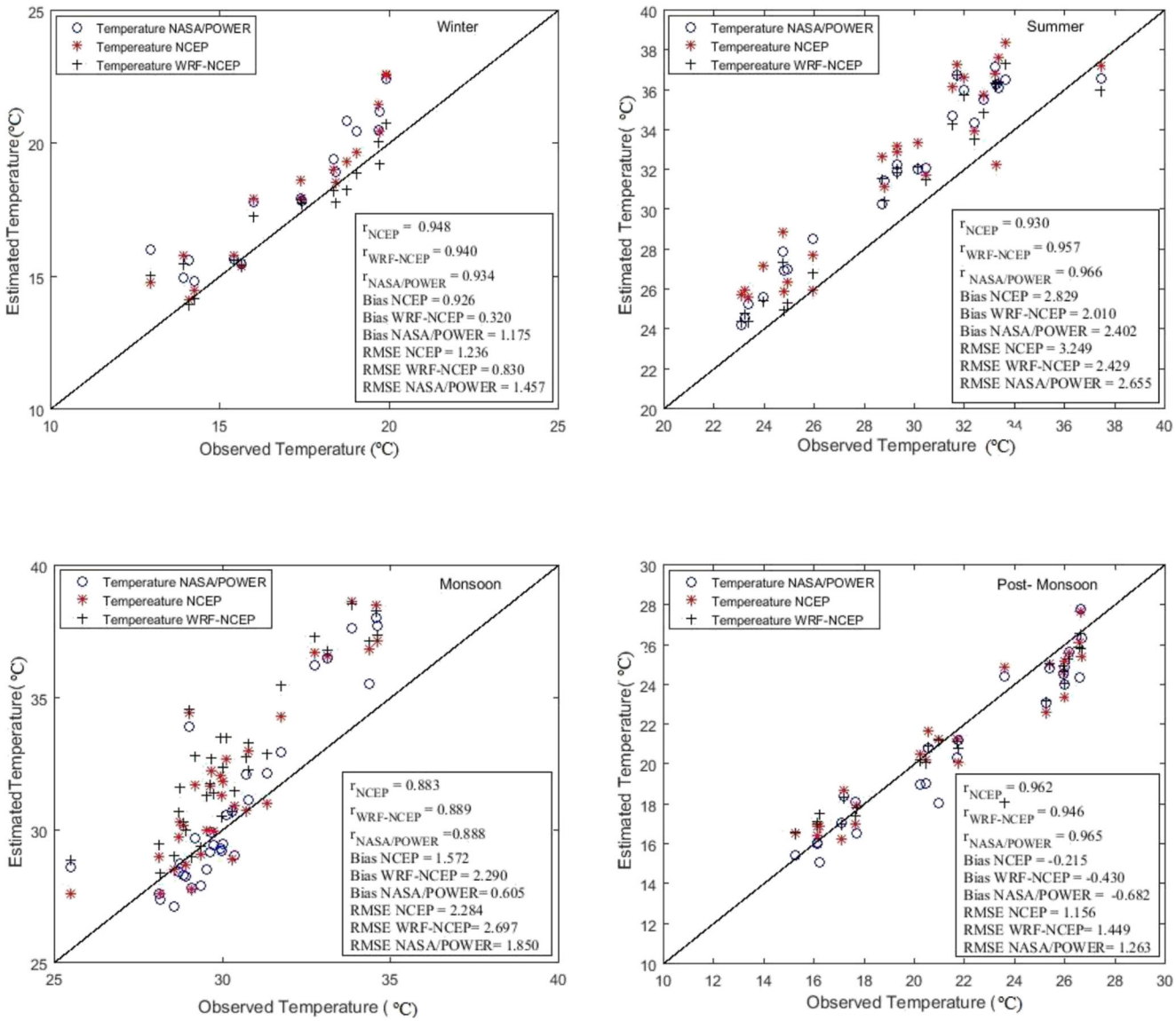

Fig. 4 Scatter plot representing the seasonal variations in temperature estimated from NCEP, WRF-NCEP, NASA/POWER, and observed data

continents, could be one of the reasons for the poor performance of estimated temperature in the monsoon season. Finally, the post-monsoon season reflects a better performance in terms of both *r* and bias when compared to the summer and monsoon periods. Overall, in winter and summer, the WRF-NCEP has shown the best results followed by NCEP and NASA/POWER; however, in monsoon and post-monsoon seasons, NASA/POWER has a much better performance as compared to the WRF-NCEP and NCEP datasets.

The seasonal analysis of temperature over the study area is shown in Fig. 5. The box and whisker diagrams are used to show the overall distribution of the datasets. The main advantage of the box and whisker plot is that it represents the distribution of data in terms of maximum, minimum, median, and both the upper and lower quartile in a single plot. The line cross across the box represents the median, while the whisker of the box showed the range of the given data sets. The winter WRF-NCEP downscaled data shows a close agreement with the observed temperature, while the NCEP and NASA/POWER show an overestimation. During the monsoon season, NASA/POWER has a good agreement with the observed median temperature. Outside this period, it is the WRF-NCEP data is in closer agreement to the observations.

3.2 Comparative assessment of evapotranspiration products

To understand the performance statistics of NCEP, WRF-NCEP, and NASA/POWER estimated ETo over the study area, the relative plot of the pooled dataset with the observed ETo is shown in Fig. 6. Results indicated that the NCEP and NASA/POWER data showed an overestimation most of the time. Higher ETo was observed for April to July months; this is due to the very high temperature in these months. According to correlation statistics, the WRF-NCEP has a marginal high correlation of 0.969 followed by NASA/POWER and NCEP with *r* value of 0.960 and 0.959 respectively. On the other hand, a high bias has been observed in the case of NCEP (0.241) followed by WRF-NCEP (0.230), and least in the case of NASA/POWER data (0.154). Even in terms of RMSE, as compared to the NCEP (0.422) and WRF-NCEP (0.402), the NASA/POWER showed a better performance with a value of 0.348. Both NCEP and WRF-NCEP estimated ETo showed an overestimation when compared with the ground data, whereas in case of NASA/POWER, it is underestimating most of the time. Overall, the NASA/POWER data showed a small discrepancy in estimation of ETo (Fig. 7).

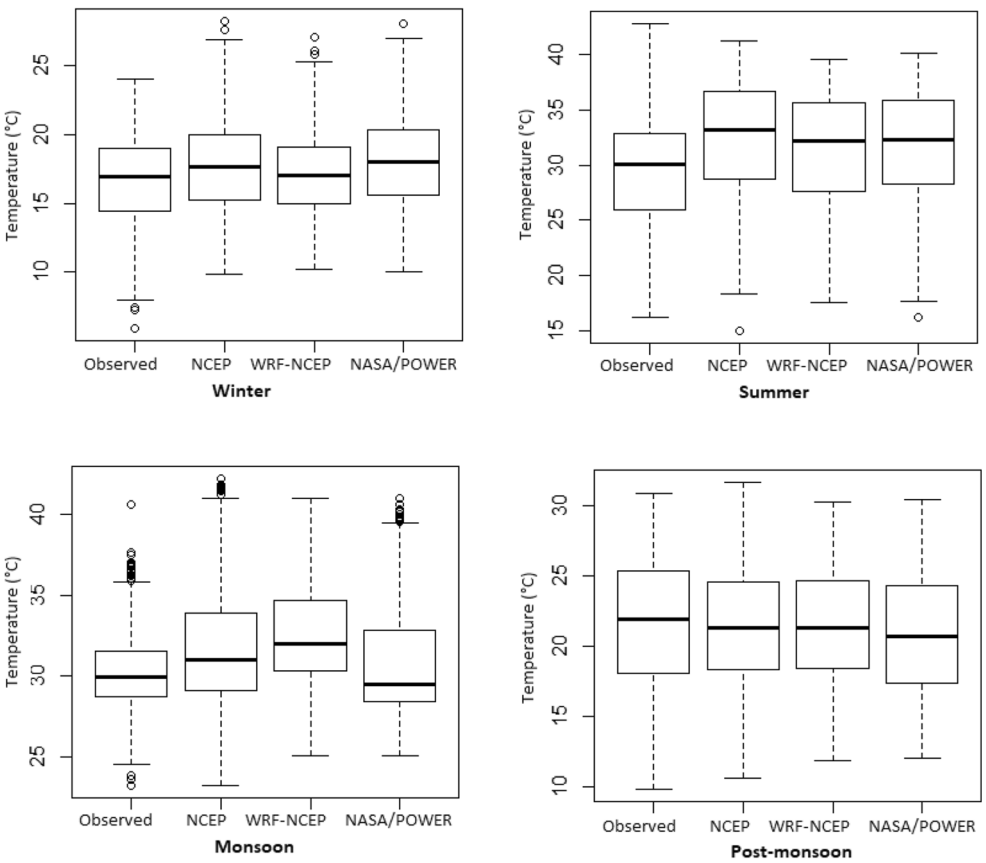

Fig. 5 Seasonal distribution of temperature over the study area

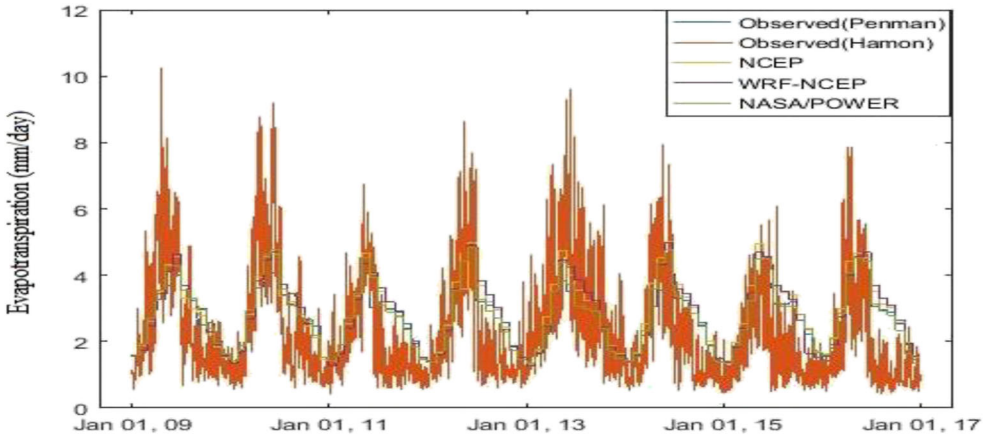

Fig. 6 Temporal plots representing the variations among NCEP, WRF-NCEP, and NASA/POWER daily ETo (estimated using Hamon's method) with observed data

3.3 Seasonality assessment of ETo

The seasonal distribution of ETo was explained using the Box-whisker plots as shown in Fig. 8. As it can observed from the figures, in comparison to the other datasets, the WRF-NCEP showed a good performance with the observed ETo. Further, among the four seasons, the post-monsoon season (October, November, and December) has less variations as compared to the observed data. In the summer and monsoon seasons, the ETo is generally overestimating, while in the case of post-monsoon, it shows an underestimation. In post-monsoon, the WRF-NCEP analyzed data showed a good agreement with the observational data. Even though the overall results are good, the output indicated poor simulation of higher ETo values throughout the period under consideration, whereas the simulation of lower ETo values are reasonably good. In Hamon's method, as temperature is the prime factor for the ETo calculation, the differences in the ETo value could be due to the poor quality of the temperature datasets.

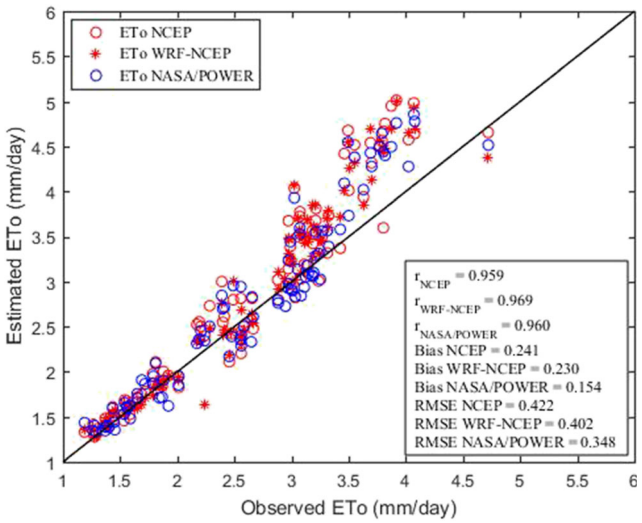

Fig. 7 Scatter plots of NCEP, WRF-NCEP, and NASA/POWER daily ETo with observed data

The scatter plot representing the seasonal variations in ETo derived from NCEP, WRF-NCEP, NASA/POWER, and observed datasets is shown in Fig. 9. The performance statistics are also calculated for the seasonal ETo and presented in Table 2. A considerable difference was found between the NASA/POWER, NCEP, and WRF-NCEP for all the four seasons. For the winter season, the values of *r*, *bias*, and *RMSE* were reported as 0.945, 0.089, and 0.121 for NCEP respectively, while for WRF-NCEP, the values of $r = 0.947$, $bias = 0.026$, and $RMSE = 0.070$ were obtained. On the other hand, for NASA/POWER, values of 0.940, 0.112, and 0.139 respectively were obtained for *r*, *bias*, and *RMSE* respectively. The results in the winter season indicated that the WRF-NCEP is performing better than the other dataset in this season. In the summer season *r*, *bias*, and *RMSE* were found as 0.908, 0.523, and 0.628 for NCEP respectively, while the WRF-NCEP revealed values of 0.936, 0.373, and 0.480 for *r*, *bias*, and *RMSE* respectively. Similarly, for NASA/POWER, the values of $r = 0.949$, $bias = 0.439$, and $RMSE = 0.511$ were obtained, which indicated that the WRF-NCEP can simulate a better ETo than the NASA/POWER and NCEP datasets. For monsoon season, *r*, *bias*, and *RMSE* (in the order) were reported as 0.896, 0.311, and 0.461 for NCEP, 0.902, 0.442, and 0.535 for WRF-NCEP, and 0.904, 0.136, and 0.373 for NASA/POWER estimated ETo respectively. Analysis revealed that during the monsoon season, NASA/POWER was found much better than the other datasets for ETo estimation. For post-monsoon season, *r*, *bias*, and *RMSE* were reported as (in the order) 0.956, − 0.034, and 0.143 for NCEP, 0.949, − 0.063, and 0.167 for WRF-NCEP, and 0.960, − 0.081, and 0.153 for NASA/POWER data respectively. The results indicated that during post-monsoon season, there is no improvement after downscaling or by using the NASA/POWER dataset as NCEP itself is giving better performance than the other two datasets. This indicate that a better parametrization scheme or combination of different parametrization schemes is needed in WRF for simulation of temperature during post-monsoon season. In the seasonal analysis, for summer and winter seasons, the WRF-NCEP

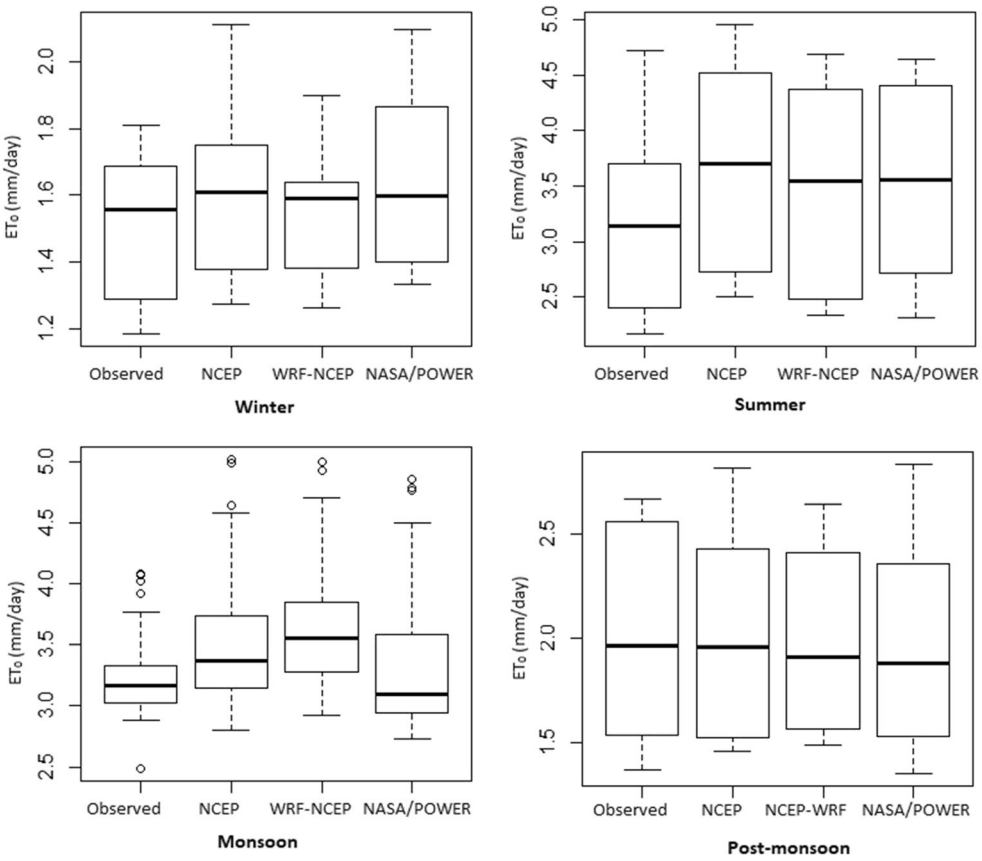

Fig. 8 Seasonal distribution of ETo over the study area

estimated ETo yields a lower RMSE than the NCEP and NASA/POWER data and show a very close agreement with the observed dataset. However, due to better capture of physics especially by WRF during monsoon season, a more accurate ETo simulation was obtained, as a high performance was obtained in the pooled dataset. The results indicated that as the performances of WRF-NCEP and NASA/POWER-based ETo are very close, any of them can be used for the ETo estimation. However, as WRF-NCEP requires high-performance computing facility and based on complex physics, NASA/POWER could be a better choice for different applications, as it can be directly obtained from the provider.

3.4 Comparison with the Penman-Monteith estimated ETo

For calculation of ETo using the Penman-Monteith method, the dataset of wind speed, solar radiation, relative humidity, and air temperature were taken into account, obtained from the ground-based meteorological station. Penman-Monteith method is now a globally accepted method for calculation of ETo and can be used here to check the performances of different ETo products. The ETo obtained from Penman-Monteith method is used as benchmark to evaluate the results of the WRF-NCEP, NASA/POWER, and NCEP-based ETo calculated using the Hamon's method and the results are shown through the Taylor diagram (Fig. 10). Taylor diagram is an integrated way of showing the performances in terms of correlation, deviation, and RMSE using a single diagram. The circle mask in the *x*-axis is the reference point, represent the ETo estimated from Penman-Monteith's methods, whereas the position of the different labels reflects the statistical characteristics of the different model data with the observed one. In the figure, it showed that the NASA/POWER has maximum agreement with the observed data in terms of correlation, RMSE, and deviation followed by WRF-NCEP and NCEP. Therefore, from the overall performance, the NASA/POWER has shown the skillful results in estimation of ETo over the study area.

4 Conclusions

Despite the prime importance of evapotranspiration in various hydrometeorological application, it is not often possible to assess evapotranspiration from ground-based weather station. An alternative to this is the use of various reanalysis global datasets and use of mesoscale model for downscaling the global reanalysis data for ungauged sites to estimate ETo. However, there are not many well-documented studies available in the literature to show the performance of the NCEP (with WRF downscaling) and NASA/POWER for ETo

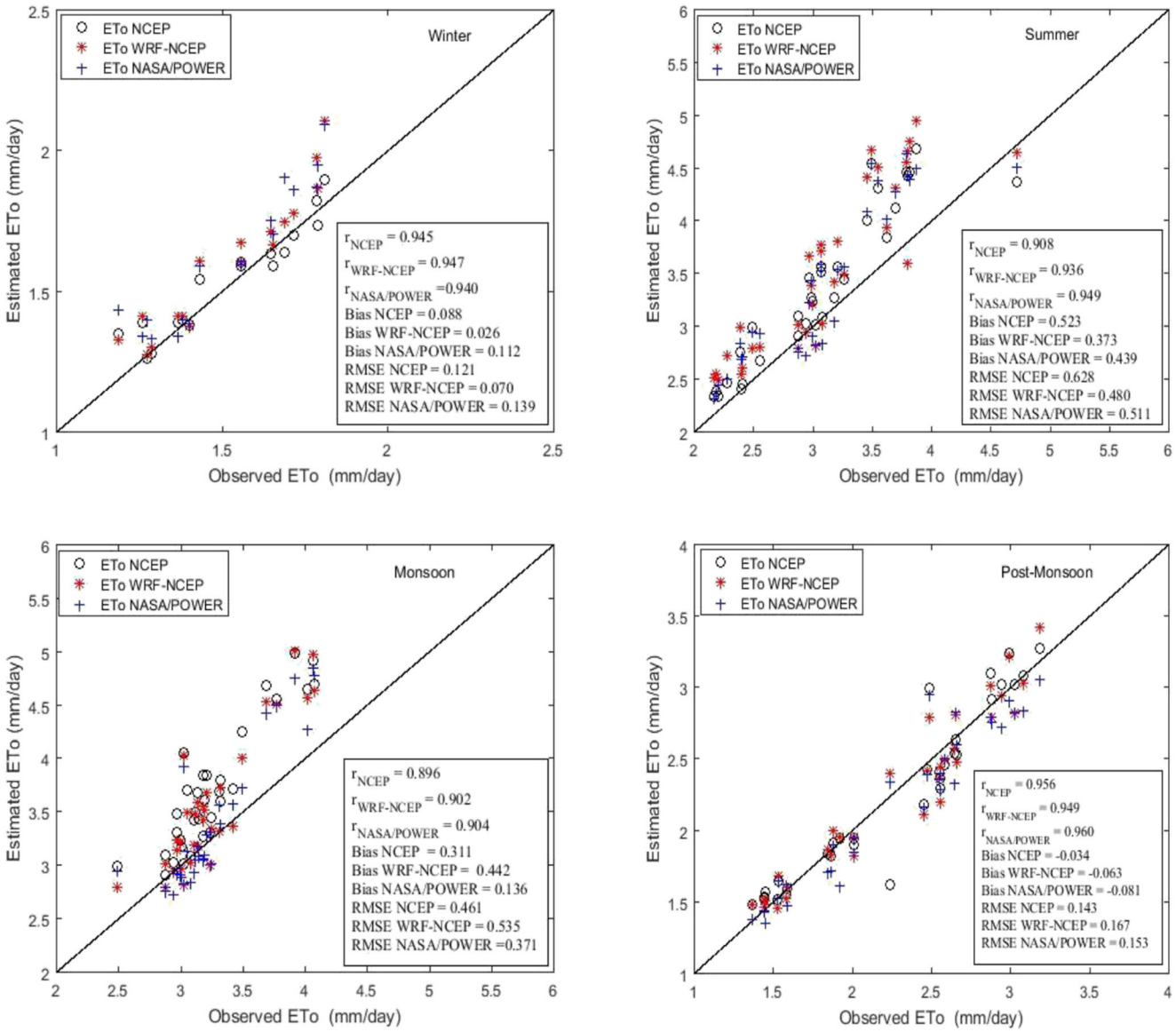

Fig. 9 Scatter plots representing seasonal variations in ETo estimated from NCEP, WRF-NCEP, NASA/POWER, and observed data

estimation, especially for the Indian regions. In this study, an attempt has been made to evaluate the performance of various global reanalysis datasets and the capability of WRF model in estimating evapotranspiration over an agricultural field. Therefore, this paper provides a detailed cross comparison of ETo estimated from different existing datasets—NCEP, WRF downscaled NCEP, and NASA/POWER over cropland by using Hamon's and Penman-Monteith's methods. In order to check the performances of different datasets, the WRF model was used to downscale the global NCEP data into much

Table 2 Performance statistics for the seasonal and pooled daily ETo

ETo	NCEP			WRF-NCEP			NASA/POWER		
	r	RMSE	Bias	*r*	RMSE	Bias	*r*	RMSE	Bias
Pooled	0.959	0.422	0.241	0.969	0.402	0.230	0.960	0.348	0.154
Winter	0.945	0.121	0.089	0.947	0.070	0.026	0.940	0.139	0.112
Summer	0.908	0.628	0.523	0.936	0.480	0.373	0.949	0.511	0.439
Monsoon	0.896	0.461	0.311	0.902	0.535	0.442	0.904	0.373	0.136
Post-monsoon	0.956	0.143	− 0.034	0.949	0.167	− 0.063	0.960	0.153	− 0.081

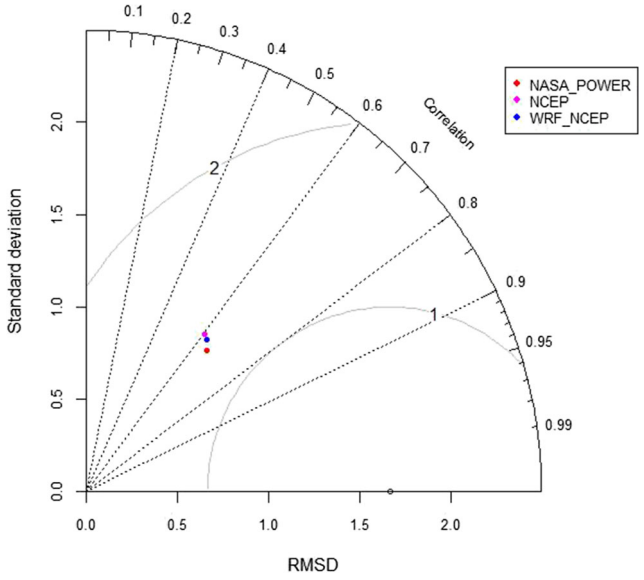

Fig. 10 Performance of the NASA_POWER, NCEP, and WRF-NCEP estimated ETo with the Penman-Monteith-based ETo as benchmark

finer resolution. The accuracy and seasonal performance of ETo estimated from three globally products NCEP global reanalysis and WRF downscaled and NASA/POWER were compared with the ground-based measurements. The temperature variable is used for the estimation of ETo using the Hamon's method on both annual and seasonal basis. Based on the results, the NASA/POWER and WRF-NCEP estimated ETo using Hamon's method is giving accurate result and showed a close match with the ground-based dataset. The ETo values calculated using the different datasets and Hamon's method were compared against the Penman-Monteith method as well, which also showed a close agreement of the ETo calculated from different global dataset with the observed one. Overall, the NASA/POWER showed a close agreement with the observed dataset in terms of bias and RMSE, which indicates that the NASA/POWER is good to use for different applications as it needs less calculation in comparison to WRF that needs sophisticated schemes and requires high power computing system. The outcomes of the study could be helpful in assessing the reliability of the NCEP, WRF downscaled NCEP, and NASA/POWER data for various hydrometeorological applications. Further, this study can improve forecasting application and effectiveness of hydrometeorological modeling especially for the ungauged areas.

Acknowledgments The authors would like to thank the SERB-DST for funding this research and DST-Mahamana Centre for Excellence in Climate Change Research, Institute of Environment and Sustainable Development, Banaras Hindu University, for providing necessary support for this research. The authors would like to thank the National Centers for Environmental Prediction for providing the NCEP data and NASA Langley Research Center (LaRC) POWER Project for providing NASA-POWER datasets. The authors are also thankful to the Institute of Agricultural Sciences, Banaras Hindu University, for providing ground-based observational datasets.

References

http://imd.gov.in/section/nhac/wxfaq.pdf

Alkaeed O, Flores C, Jinno K, Tsutsumi A (2006) Comparison of several reference evapotranspiration methods for Itoshima Peninsula area, Fukuoka, Japan Memoirs of the Faculty of Engineering, Kyushu University 66:1–14

Allen RG, Pereira LS, Raes D, Smith M (1998) Crop evapotranspiration-guidelines for computing crop water requirements-FAO Irrigation and drainage paper 56 Fao. Rome 300:D05109

Cai J, Liu Y, Lei T, Pereira LS (2007) Estimating reference evapotranspiration with the FAO Penman–Monteith equation using daily weather forecast messages. Agric For Meteorol 145:22–35

Cai X, Wang D, Laurent R (2009) Impact of climate change on crop yield: a case study of rainfed corn in central Illinois. J Appl Meteorol Climatol 48:1868–1881

Chen D, Gao G, Xu C-Y, Guo J, Ren G (2005) Comparison of the Thornthwaite method and pan data with the standard Penman-Monteith estimates of reference evapotranspiration in China. Clim Res 28:123–132

Djaman K et al (2015) Evaluation of sixteen reference evapotranspiration methods under sahelian conditions in the Senegal River Valley. J Hydrol: Reg Stud 3:139–159

Dudhia J (1988) Numerical study of convection observed during the winter monsoon experiment using a mesoscale two-dimensional model. J Atmos Sci 46:3077–3107. https://doi.org/10.1175/1520-0469(1989)046<3077:NSOCOD>2.0.CO;2

Falk M et al (2014) Evaluated crop evapotranspiration over a region of irrigated orchards with the improved ACASA–WRF model. J Hydrometeorol 15:744–758

Hamon WR (1960) Estimating potential evapotranspiration. Massachusetts Institute of Technology

Hong S-Y, Lim J-OJ (2006) The WRF single-moment 6-class microphysics scheme (WSM6). J Korean Meteor Soc 42:129–151

Ishak AM, Bray M, Remesan R, Han D (2010) Estimating reference evapotranspiration using numerical weather modelling. Hydrol Process 24:3490–3509

Kalnay E et al (1996) The NCEP/NCAR 40-year reanalysis project. Bull Am Meteorol Soc 77:437–472

Kar SK, Nema A, Singh A, Sinha B, Mishra C (2016) Comparative study of reference evapotranspiration estimation methods including Artificial Neural Network for dry sub-humid agro-ecological region. J Soil Water Conserv 15:233–241

Kim H-J, Wang B (2011) Sensitivity of the WRF model simulation of the East Asian summer monsoon in 1993 to shortwave radiation schemes and ozone absorption. Asia-Pac J Atmos Sci 47:167–180

Lang D et al (2017) A comparative study of potential evapotranspiration estimation by eight methods with FAO Penman–Monteith method in Southwestern China. Water 9:734

Lin P et al (2018) Spatiotemporal evaluation of simulated evapotranspiration and streamflow over Texas using the WRF-hydro-RAPID modeling framework. JAWRA J Am Water Resour Assoc 54:40–54

Mall R, Gupta B (2002) Comparison of evapotranspiration models. Mausam 53:119–126

McCabe GJ, Hay LE, Bock A, Markstrom SL, Atkinson RD (2015) Inter-annual and spatial variability of Hamon potential evapotranspiration model coefficients. J Hydrol 521:389–394

Mlawer EJ, Taubman SJ, Brown PD, Iacono MJ, Clough SA (1997) Radiative transfer for inhomogeneous atmospheres: RRTM, a validated correlated-k model for the longwave. J Geophys Res: Atmos 102:16663–16682

Mohan M, Sati AP (2016) WRF model performance analysis for a suite of simulation design. Atmos Res 169:280–291

Monteith J (1965) Evaporation and environment. pp. 205–234. In GE Fogg Symposium of the Society for Experimental Biology The State and Movement of Water in Living Organisms 19

Nag A, Adamala S, Raghuwanshi N, Singh R, Bandyopadhyay A (2014) Estimation and ranking of reference evapotranspiration for different spatial scale in India vol 34

Pandey PK, Dabral PP, Pandey V (2016) Evaluation of reference evapotranspiration methods for the northeastern region of India. Int Soil Water Conserv Res 4:52–63

Penman H (1956) Estimating evaporation: transactions. Am Geophys Union 39:19–56

Petropoulos G, Ireland G, Cass A, Srivastava P (2015) Performance assessment of the SEVIRI evapotranspiration operational product: results over diverse Mediterranean ecosystems. IEEE Sensors. https://doi.org/10.1109/jsen20152390031

Petropoulos GP et al (2016) Operational evapotranspiration estimates from SEVIRI in support of sustainable water management. Int J Appl Earth Observ Geoinformation 49:175–187

Podder S, Khan RS, Mohon SMAA, Hussain MJ, Basher E Solar radiation approximation using sunshine hour at patenga, Bangladesh. In: Electrical and Computer Engineering (ICECE), 2014 International Conference on, 2014. IEEE, pp 321–324

Schwartz CS et al (2009) Next-day convection-allowing WRF model guidance: a second look at 2-km versus 4-km grid spacing. Mon Weather Rev 137:3351–3372

Silva D, Meza FJ, Varas E (2010) Estimating reference evapotranspiration (ETo) using numerical weather forecast data in central Chile. J Hydrol 382:64–71

Skamarock WC, Klemp JB, Dudhia J (2001) Prototypes for the WRF (Weather Research and Forecasting) model. In: Preprints, Ninth Conf. Mesoscale Processes, J11–J15, Amer. Meteorol. Soc., Fort Lauderdale, FL

Srivastava PK, Han D, Rico Ramirez MA, Islam T (2013) Comparative assessment of evapotranspiration derived from NCEP and ECMWF global datasets through Weather Research and Forecasting model. Atmos Sci Lett 14:118–125

Srivastava PK, Han D, Islam T, Petropoulos GP, Gupta M, Dai Q (2016) Seasonal evaluation of evapotranspiration fluxes from MODIS satellite and mesoscale model downscaled global reanalysis datasets. Theor Appl Climatol 124:461–473

Srivastava PK, Han D, Yaduvanshi A, Petropoulos GP, Singh SK, Mall RK, Prasad R (2017) Reference evapotranspiration retrievals from a mesoscale model based weather variables for soil moisture deficit estimation. Sustainability 9:1971

Thornthwaite CW (1948) An approach toward a rational classification of climate. Geogr Rev 38:55–94. https://doi.org/10.2307/210739

Zotarelli L, Dukes MD, Romero CC, Migliaccio KW, Morgan KT (2010) Step by step calculation of the Penman-Monteith evapotranspiration (FAO-56 method) Institute of Food and Agricultural Sciences University of Florida